ELSEVIER

Journal of Power Sources 113 (2003) 44–56

JOURNAL OF POWER SOURCES

www.elsevier.com/locate/jpowsour

A simple model for interconnect design of planar solid oxide fuel cells

Cameron W. Tanner, Anil V. Virkar*

Department of Materials Science and Engineering, University of Utah, 304 EMRO, 122 South Central Campus Drive, Salt Lake City, UT 84112-0560, USA

Received 21 August 2002; accepted 3 September 2002

Abstract

Two geometries of solid oxide fuel cells (SOFCs) are currently under development, tubular and planar. Both types of cells are configured in a stack using an interconnect, which electrically connects the anode of one cell to the cathode of the adjacent cell, while also physically isolating fuel from oxidant. Proper design of the interconnect in conjunction with single-cells is critical to minimizing the overall stack resistance. This work quantitatively examines the dependence of total SOFC stack resistance as a function of interconnect contact spacing, interconnect contact area, cathode thickness, electrolyte thickness, anode thickness, and transport properties associated with each region and at interfaces (charge transfer resistance). Both one-dimensional (channels) and two-dimensional (dimples) symmetries of interconnect geometry are analyzed for planar cells. Analytical expressions are derived for the area-specific resistance (ASR) of a repeat unit consisting of a cell and interconnect, for both geometries, as a function of cell parameters, interconnect contact area and interconnect contact spacing. It is found that the one-dimensional interconnect symmetry leads to lower values of stack-repeat unit area-specific resistance (ASR) than the two-dimensional symmetry. Thus, based on the analysis presented here the one-dimensional interconnect geometry is preferred over the two-dimensional one.

Keywords: Planar; Solid oxide fuel cell; Geometry

1. Introduction

The performance of solid oxide fuel cells (SOFCs) at the single-cell level has been improved dramatically through the use of thin electrolytes and porous composite electrodes. With techniques such as dip-coating, slurry coating, tape casting, and electrochemical vapor deposition (EVD), it is possible to fabricate gas-tight yttria-stabilized zirconia (YSZ) electrolytes of thickness in the range of 5–30 μm, which have a very low area-specific resistance at temperatures $\geq$700 °C [1–3]. Porous composite electrodes, which are mixtures of electrocatalyst and electrolyte materials, or single-phase, mixed ionic–electronic conducting (MIEC) materials, have been shown to significantly reduce the area-specific resistance associated with charge transfer (activation) reactions, both theoretically and experimentally [4–6]. Theoretically, the effective charge transfer resistance of a porous composite electrode is minimized for relatively thick electrodes (several micrometers) with a fine microstructure, in the immediate vicinity of the electrolyte [3,6]. Single-cells consisting of: (1) a porous Ni + YSZ anode of thickness ~500–1000 μm, (2) a dense electrolyte of YSZ of thickness ~5–15 μm, and (3) a porous Sr-doped $LaMnO_3$ (LSM) + YSZ cathode of thickness ~100 μm typically exhibit power densities (area-specific resistances) of ~0.8 W/cm^2 (~0.31 Ω cm^2) and ~1.5 W/cm^2 (0.17 Ω cm^2) at 700 and 800 °C, respectively. Both the cathode and the anode are often compositionally and microstructurally graded through the thickness. Near the electrolyte/electrode interface, the electrode microstructure is generally fine, and this region may exhibit mixed ionic–electronic conductivity. Away from the interface, the electrode usually has high porosity, the microstructure is usually coarse, and the conduction mechanism is predominantly electronic.

For the purpose of practical power generation, several single-cells must be connected in a stack to achieve a sufficiently high power, and build the desired voltage. In a SOFC stack, the single-cells are electrically joined with interconnects. Ideally, the power generating capacity of the stack should be the sum of capacities of the individual cells. However, there are resistances associated with interconnect

* Corresponding author. Tel.: +1-801-581-5396; fax: +1-801-581-4816.
E-mail address: anil.virkar@m.cc.utah.edu (A.V. Virkar).

0378-7753/02/$ – see front matter
PII: S0378-7753(02)00479-2

Nomenclature

E	Nernst potential (V)
I_{I}	total current for the one-dimensional interconnect design (A/cm^2)
I_{II}	total current for the two-dimensional interconnect design (A/cm^2)
L	center-to-center spacing between nearest interconnect contacts for the one-dimensional geometry (cm)
M	center-to-center spacing between nearest interconnect contacts for the two-dimensional geometry (cm)
r	radial position measured from the center of an interconnect contact (cm)
r_0	radius of the interconnect contact with the electrodes (cm)
R	area-corrected spacing between interconnect contacts for the two-dimensional geometry when circles are used instead of hexagons as the in-plane repeat unit (cm)
R_{I}	overall area-specific resistance of a repeat unit for the one-dimensional interconnect design (Ω cm^2)
R_{II}	overall area-specific resistance of a repeat unit for the two-dimensional interconnect design (Ω cm^2)
$R^{\mathrm{a}}_{\mathrm{ct}}$	charge transfer resistance at the interface of the electrolyte and a composite anode (Ω cm^2)
$R^{\mathrm{a}}_{\mathrm{ct(0)}}$	intrinsic charge transfer resistance at the interface of the electrolyte (e.g. YSZ) and the electrocatalyst (e.g. Ni), for the given particle size and volume fraction (Ω cm^2)
$R^{\mathrm{c}}_{\mathrm{ct}}$	charge transfer resistance at the interface of the electrolyte and a composite cathode (Ω cm^2)
$R^{\mathrm{c}}_{\mathrm{ct(0)}}$	intrinsic charge transfer resistance at the interface of the electrolyte (e.g. YSZ) and the electrocatalyst (e.g. LSM), for the given particle size and volume fraction (Ω cm^2)
t_{a}	thickness of the anode (cm)
t_{c}	thickness of the cathode (cm)
t_{e}	thickness of the electrolyte (cm)
$v_{\mathrm{I}}(x)$	electrostatic potential between the cathode and the anode as a function of position for the one-dimensional interconnect design for $x_0 \le x \le L/2$ (V)
$v_{\mathrm{II}}(r)$	electrostatic potential between the cathode and the anode as a function of position for the two-dimensional interconnect design for $r_0 \le r \le R/2$ (V)
x	horizontal position measured from the center of an interconnect contact (cm)
x_0	half-width of the interconnect contact with the electrodes (cm)

Greek letters

ϕ^0	electrostatic potential maintained at the cathode interconnect contact relative to the anode interconnect contact (V)
$\phi^{\mathrm{a}}_{\mathrm{I}}(x)$	electrostatic potential as a function of position within the anode for the one-dimensional interconnect design for $x \le x \le L/2$ (V)
$\phi^{\mathrm{c}}_{\mathrm{I}}(x)$	electrostatic potential as a function of position within the cathode for the one-dimensional interconnect design for $x_0 \le x \le L/2$ (V)
$\phi^{\mathrm{a}}_{\mathrm{II}}(r)$	electrostatic potential as a function of position within the anode for the two-dimensional interconnect design for $r_0 \le r \le R/2$ (V)
$\phi^{\mathrm{c}}_{\mathrm{II}}(r)$	electrostatic potential as a function of position within the cathode for the two-dimensional interconnect design for $r_0 \le r \le R/2$ (V)
ρ_{a}	electronic resistivity of the anode (Ω cm)
ρ_{c}	electronic resistivity of the cathode (Ω cm)
ρ_{e}	ionic resistivity of the electrolyte (Ω cm)
$\rho^{\mathrm{c}}_{\mathrm{e}}$	ionic resistivity of the cathode (e.g. that of YSZ in the cathode) (Ω cm)

material and interconnect design parameters. As a result, the power generating capacity of a stack is less than the sum of the capacities of single-cells. Therefore, an efficient interconnect design is of paramount importance. Some of the parameters which influence the resistance contributed by the interconnect can be deduced by considering the current path for electrons. Fig. 1 shows a schematic of a SOFC cell-interconnect repeat unit and the regions of contact with interconnect. Current flows from the electrocatalyst–electrolyte interface, through the electronically conductive electrocatalyst, such as LSM in the cathode, to interconnect. Usually, the resistance of interconnect can be assumed to be small; although this would not be the case if a resistive oxide scale forms on the interconnect. The overall resistance also depends upon the spacing between the interconnect contacts due to the resistances associated with the two electrodes and the electrolyte comprising the cell. In fact, parameters related to the electrodes, which are not formally part of interconnect, influence the effective stack resistance. For this reason, the design of interconnect is influenced by the properties of the single-cell. That is, the single-cell and interconnect should be designed as a subsystem and not as independent entities.

Several numerical models for solid oxide fuel cell stacks have been developed, which include an interconnect [7]. Ahmed et al. modeled a planar, monolithic cell [8]. The model addresses the effects of fuel utilization and heat generation on the average current density, but it does not include resistance to distribution of current in or over the electrodes parallel to the electrolyte. Bessette et al. developed a finite-element model of the tubular Siemens–Westinghouse design, which treats current distribution losses in the electrodes with a resistor network [9]. Local current

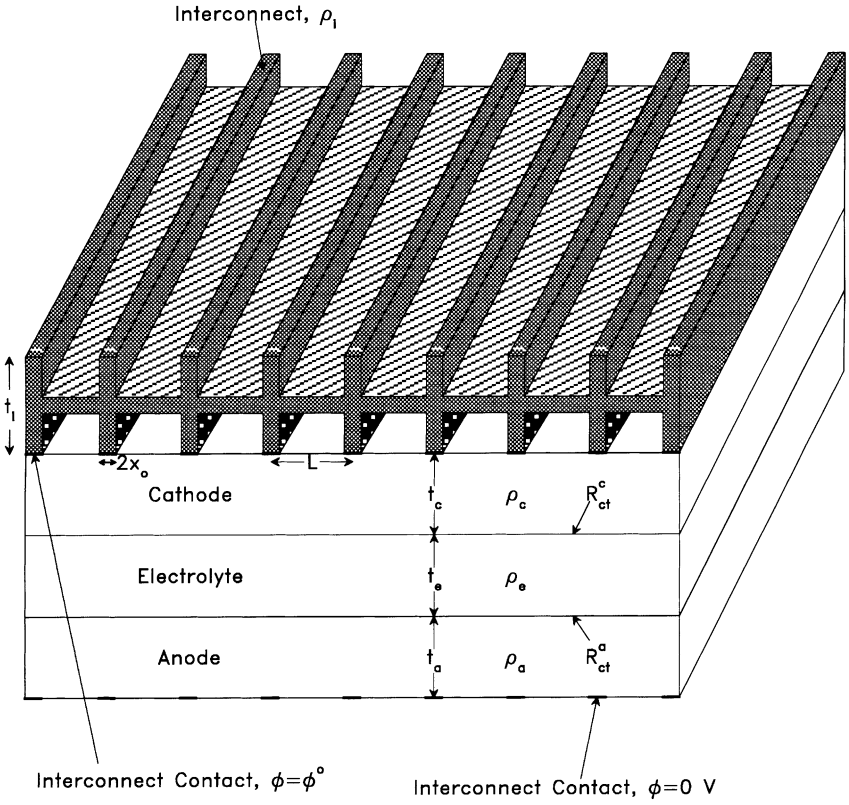

Fig. 1. A schematic of a SOFC in series contact with interconnect of one-dimensional geometry.

density was calculated as a function of axial position and angle. Local current density was noted to be nearly a factor of three higher where the interconnect contacts the electrode than midway between contacts, regardless of the axial position. Resistance to radial distribution of current in the LSM cathode was found to be very high. Effects of reduction of tube radius or changes in thickness of the electrodes, however, were not discussed. In general, the role of various parameters of the interconnect design is difficult to visualize with numerical models, except in selected cases.

The purpose of this work is to present analytical expressions, which describe the dependence of the area-specific resistance (ASR) of a SOFC stack-repeat unit, consisting of a cell and an interconnect, as a function of the cathode and anode thicknesses, charge transfer resistances (activation polarization) at the cathode–electrolyte and anode–electrolyte interfaces, ionic resistivity of the electrolyte, electronic resistivities of the anode and the cathode, respectively, distance between interconnect contacts, and interconnect–electrode contact area. The analysis treats both one- and two-dimensional interconnect symmetries. The area-specific resistance (ASR) will be used as the figure of merit to assess the design of a repeat unit consisting of a single-cell and interconnect. It will not be the objective of this paper to include temperature variations or the effects of fuel utilization. This will be the subject of a future investigation.

2. Analysis

There are two basic interconnect symmetries, which are used in planar SOFC stacks, one-dimensional (channels) and two-dimensional (dimples). Fig. 1 shows an SOFC cell-interconnect repeat unit with a one-dimensional interconnect symmetry. The interconnect contacts of width $2x_0$ are periodically spaced at a distance of L, and their length extends across the entire cell. Similarly, Fig. 2 shows another SOFC cell-interconnect repeat unit with a two-dimensional interconnect symmetry. The interconnect contacts are circular in shape and are placed in a hexagonal array to cover the surface of the electrode. The center-to-center distance between nearest neighbor interconnect contacts, as shown in the figure, is M; and the contact area per contact with the electrode is πr_0^2.

The main objective of this analysis is to calculate the area-specific resistance per repeat unit consisting of a cell and interconnect for both interconnect designs. Once this is obtained, the stack resistance is determined by simply multiplying the area-specific resistance of the repeat unit by the number of cells in the series-connected stack and dividing by the active area per cell. It is assumed at the outset that all transport properties are ohmic. Non-ohmic transport can be treated, but this would require numerical solution of the steady-state transport equations. It is also assumed that transport of gaseous species to and from the

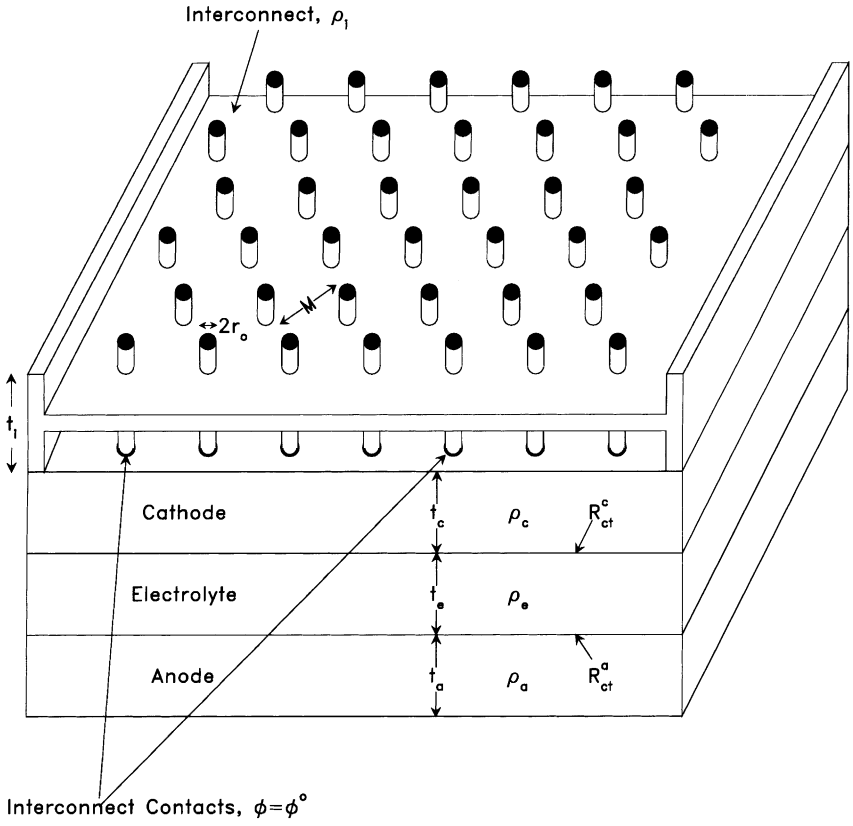

Fig. 2. A schematic of a SOFC in series contact with interconnect of a two-dimensional geometry.

electrodes, as well as through the electrodes, is fast. That is, concentration polarization is assumed to be negligible. These assumptions are justifiable for two reasons: (1) the current versus voltage response of SOFCs (in stacks) is usually nearly linear, and (2) it has been shown, both theoretically and experimentally, that concentration polarization becomes significant only for thick electrodes (>1 mm) operating at high current densities.

In a steady-state, the divergence of the flux of each species is zero, and for spatially invariant, ohmic transport properties, this leads to the result that the electrostatic potential within all regions of a SOFC must satisfy the Laplace equation, $\nabla^2\phi = 0$.[1] In principle, the Laplace equation should be solved subject to appropriate boundary conditions within each region of the SOFC (cathode, electrolyte, and anode). The complexity of the boundary conditions and number of regions of various materials, make analytic expressions for the area-specific resistance based upon solutions to Laplace equations difficult. Analytic expressions, however, can be obtained using a ladder network approach if two assumptions are made. (1) The electrostatic potential within the electrocatalyst materials of the cathode and anode is invariant in the vertical direction, namely, $\partial\phi/\partial y = 0$. This is justified if the resistivities of the electrodes are much smaller than that of the electrolyte. In a SOFC, the materials used for the electrocatalysts in the cathode (LSM, $\rho_c = 0.01\ \Omega$ cm and anode $\rho_a = 0.001\ \Omega$ cm) have resistivities that are significantly lower than that of the electrolyte (eight YSZ, $\rho_e = 50\ \Omega$ cm). (2) In the electrolyte, the electrostatic potential exhibits a much greater variation through the thickness rather than along the plane of the electrolyte, i.e. $\partial\phi/\partial y \gg \partial\phi/\partial x$. Since the resistivities of the electrocatalyst materials in a SOFC are rather small, the electrostatic potentials in the cathode and the anode vary slowly in the horizontal (in-plane) direction. Since the electrolyte lies between the cathode and the anode, the electrostatic potential within the electrolyte varies slowly in the horizontal direction, as well. This implies that current flows from the anode to the cathode through the electrolyte primarily in the vertical (through the thickness) direction.

2.1. One-dimensional interconnect symmetry

The one-dimensional stack-repeat unit used for the analysis is shown in Fig. 3. The potentials at the interconnect–electrode interfaces are fixed. Currents are shown entering and leaving differential elements within the cathode and the anode. In steady-state, currents entering and leaving any

[1] This assumes that each region is locally homogeneous and a continuum, and that electrochemical reactions are confined to thin regions at electrolyte/electrode interfaces.

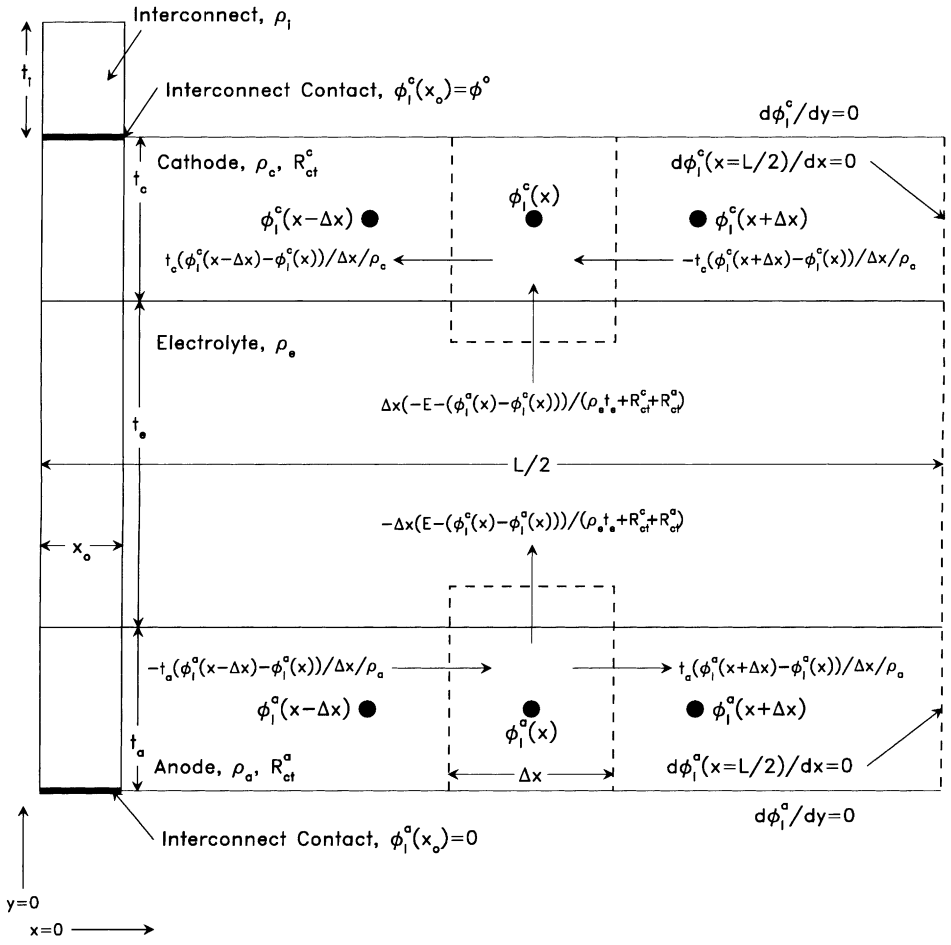

Fig. 3. A schematic showing a cross-section of the SOFC depicted in Fig. 1. This view is obtained by considering the symmetry associated with the periodically repeated one-dimensional interconnect geometry.

differential element must be conserved. This condition for an element in the cathode gives

$$-\frac{t_c}{\rho_c}\left[\frac{\phi_I^c(x+\Delta x)-\phi_I^c(x)}{\Delta x}\right]-\frac{t_c}{\rho_c}\left[\frac{\phi_I^c(x-\Delta x)-\phi_I^c(x)}{\Delta x}\right]+\left[\frac{\Delta x}{\rho_e t_e+R_{ct}^c+R_{ct}^a}\right](-E-\phi_I^a(x)+\phi_I^c(x))=0 \quad (1)$$

The parameters in this equation are: the position measured horizontally from the center of the interconnect contact, x; the electrostatic potential in the cathode as a function of position, $\phi_I^c(x)$; the electrostatic potential in the anode as a function of position, $\phi_I^a(x)$; the thickness of the cathode, t_c; the thickness of the electrolyte, t_e; the thickness of the anode t_a; the electronic resistivity of the cathode (assumed for the moment to be constant through the thickness), ρ_c; the ionic resistivity of the electrolyte, ρ_e; the electronic resistivity of the anode (assumed to be constant through the thickness), ρ_a; the charge transfer resistance at the cathode–electrolyte interface, R_{ct}^c; the charge transfer resistance at the anode–electrolyte interface, R_{ct}^a; and the Nernst potential, E. Although for the purposes of simplifying the analysis, the charge transfer resistances are given as being associated with the physically distinct electrode–electrolyte interfaces, it can be shown that the charge transfer resistances themselves are functions of the electrode structure [3–6]. This aspect will be elaborated upon later. Taking the limit as $\Delta x \to 0$ of the first two terms in Eq. (1) and then dividing by Δx gives

$$-\frac{t_c}{\rho_c \Delta x}\left[\left.\frac{d\phi_I^c(x)}{dx}\right|_+-\left.\frac{d\phi_I^c(x)}{dx}\right|_-\right]+\frac{-E-\phi_I^a(x)+\phi_I^c(x)}{\rho_e t_e+R_{ct}^c+R_{ct}^a}=0 \quad (2)$$

Again, taking the limit as $\Delta x \to 0$ and rearranging terms gives

$$-\frac{d^2\phi_I^c(x)}{dx^2}+k_c[-E-\phi_I^a(x)+\phi_I^c(x)]=0 \quad (3)$$

where

$$k_c=\frac{\rho_c/t_c}{\rho_e t_e+R_{ct}^c+R_{ct}^a} \quad (4)$$

If the cathode is graded such that the electronic conductivity is a function of through the thickness, the ρ_c from the above

equations is replaced by the cathode resistivity, $\langle\rho_c\rangle$, given by

$$\langle\rho_c\rangle = \frac{t_c}{\int_0^{t_c} dy/\rho_c(y)} \tag{5}$$

where $\rho_c(y)$ is the electronic resistivity of the cathode at a position y, measured with respect to one of the interfaces; cathode/electrolyte interface, or cathode/oxidant gas phase interface. For a graded anode, similar average value of anode resistivity, $\langle\rho_a\rangle$, can be defined. Differential Eq. (3) describes the spatial dependence of the electrostatic potential within the cathode in the range $x_0 \le x \le L/2$ for the one-dimensional interconnect symmetry. There are two unknowns in Eq. (3), namely, the electrostatic potentials within the cathode and the anode, as functions of position. In order to solve Eq. (3), the spatial dependence of the electrostatic potential within the anode must also be evaluated. In steady-state, the current within a differential element in the anode must also be conserved (see Fig. 3). Repeating the same procedure, as was used for the cathode, gives

$$\frac{-d^2\phi_I^a(x)}{dx^2} + k_a[E - \phi_I^c(x) + \phi_I^a(x)] = 0 \tag{6}$$

where

$$k_a = \frac{\rho_a/t_a}{\rho_e t_e + R_{ct}^c + R_{ct}^a} \tag{7}$$

In the case of anode of graded properties, ρ_a from the above equations is replaced by $\langle\rho_a\rangle$ which is defined by an equation analogous to Eq. (4). Differential Eqs. (3) and (6) are linearly independent and can, in principle, be solved simultaneously to obtain $\phi_I^c(x)$ and $\phi_I^a(x)$. In order to reduce this system of two differential equations and two unknowns to a single differential equation involving only one unknown, the following substitution will be made:

$$v_I(x) = \phi_I^c(x) - \phi_I^a(x) \tag{8}$$

Eq. (8) describes the difference in electrostatic potentials between the cathode and the anode at a given position, x. Subtracting Eq. (6) from Eq. (3), and using the above substitution gives

$$-\left[\frac{1}{k_c + k_a}\right]\frac{d^2 v_I(x)}{dx^2} + v_I(x) = E \tag{9}$$

The solution to this differential equation is easily shown to be

$$v_I(x) = E + v_1 e^{ax} + v_2 e^{-ax} \tag{10}$$

where

$$a = \sqrt{\frac{\rho_c/t_c + \rho_a/t_a}{\rho_e t_e + R_{ct}^c + R_{ct}^a}} = \sqrt{k_c + k_a} \tag{11}$$

and v_1 and v_2 are constants, which must be determined by applying the requisite boundary conditions. The two boundary conditions applicable to the geometry of Fig. 3 are

$$v_I(x_0) = \phi^0 \quad \text{and} \quad \left.\frac{dv_I(x)}{dx}\right|_{x=L/2} = 0 \tag{12}$$

The first boundary condition corresponds to the fixed potentials at the interconnect contacts. The mirror plane at $x = L/2$ across which no current flows gives the second boundary condition (symmetry). Solving for v_1 and v_2 gives

$$v_1 = v_2 e^{-aL} \quad \text{and} \quad v_2 = \frac{\phi^0 - E}{e^{a(x_0 - L)} + e^{-ax_0}} \tag{13}$$

Substitution of Eq. (13) into Eq. (10) gives the complete solution for the difference in electrostatic potentials between the cathode and the anode, $v_I(x)$, as a function of position when, $x_0 \le x \le L/2$, namely,

$$v_I(x) = E + (\phi^0 - E)\left[\frac{e^{a(x-L)} + e^{-ax}}{e^{a(x_0-L)} + e^{-ax_0}}\right] \tag{14}$$

This equation may be used as an intermediate result to obtain solutions for $\phi_I^c(x)$ and $\phi_I^a(x)$. Alternatively, it is sufficient for the evaluation of the area-specific resistance.

Examination of Fig. 3 shows that there are two separate regions of the electrolyte that contribute to the current flow, I_I. For the inner region located directly beneath the interconnect contact, that is for $0 \le x \le x_0$, the potential difference is constant and is given by Eq. (12). From Fig. 3, the current flowing through the electrolyte in the inner region, per unit length in the z-direction (into the paper) is

$$I_I^i = \frac{(E - \phi^0)x_0}{\rho_e t_e + R_{ct}^c + R_{ct}^a} \tag{15}$$

and is over the region $0 \le x \le x_0$. In the outer region, that is, for $x_0 \le x \le L/2$, the potential difference between the cathode and the anode varies as a function of position. From Fig. 3, the current flowing through a differential element of the electrolyte is given by

$$dI_I^0 = \frac{(E - v_I(x))\,dx}{\rho_e t_e + R_{ct}^c + R_{ct}^a} \tag{16}$$

per unit length in the z-direction (into the paper). This current is found by substituting Eq. (14) into Eq. (16) and integrating from x_0 to $L/2$, and is given by

$$I_I^0 = \frac{E - \phi^0}{a(\rho_e t_e + R_{ct}^c + R_{ct}^a)}\left[\frac{e^{-ax_0} - e^{a(x_0-L)}}{e^{-ax_0} + e^{a(x_0-L)}}\right] \tag{17}$$

The net current (over the distance 0 to L) is given by the sum of Eqs. (15) and (17), that is,

$$I_I = I_I^i + I_I^0 \tag{18}$$

Evaluation of the area-specific resistance is now straightforward. The resistance of the structure shown in Fig. 3 between the interconnect contacts can be found by applying Ohm's law to the expression for the total current, i.e.

absolute value of $(d\phi^0/dI_I)$. Interconnect material acts in series and contributes approximately a resistance of $\rho_i t_i/x_0$ to the total.[2] Multiplying the total resistance by the area (per unit dimension along the channels), $L/2$, gives an analytical expression for the area-specific resistance (ASR) of the stack-repeat unit, given by

$$R_I = \frac{L}{2}\left(\frac{\rho_e t_e + R_{ct}^c + R_{ct}^a}{x_0 + (1/a)[(e^{-ax_0} - e^{a(x_0-L)})/(e^{-ax_0} + e^{a(x_0-L)})]} + \frac{\rho_i t_i}{x_0}\right) \tag{19}$$

in units of $\Omega\,cm^2$. Note that this equation is a function of the various material and design parameters.

2.2. Two-dimensional interconnect symmetry

The analysis of the two-dimensional interconnect symmetry will proceed in a manner similar to the one presented here for the one-dimensional symmetry. The repeat unit (in the plane of the interconnect) for the two-dimensional interconnect symmetry, shown in Fig. 2, is a hexagon with sides of length $M/2$. For the purpose of simplifying the mathematics, the hexagonal repeat unit will be approximated by a circle which introduces a cylindrical symmetry. The radius of this circle, $R/2$, will be chosen such that it has an area equal to that of the hexagon. The relationship between R and M is

$$R = M\left(\frac{27}{4\pi^2}\right)^{1/4} \tag{20}$$

Fig. 4 shows a circular section of a SOFC with the interconnect contact located at the center. The figure shows current entering and leaving a cylindrical ring of thickness Δr in both the cathode and the anode. In steady-state, the current entering and leaving the ring within the cathode must be conserved. This leads to

$$-\frac{2\pi t_c(r+\Delta r/2)}{\rho_c}\left[\frac{\phi_{II}^c(r+\Delta r) - \phi_{II}^c(r)}{\Delta r}\right] - \frac{2\pi t_c(r-\Delta r/2)}{\rho_c}\left[\frac{\phi_{II}^c(r-\Delta r) - \phi_{II}^c(r)}{\Delta r}\right] + \frac{\pi(r+\Delta r/2)^2 - \pi(r-\Delta r/2)^2}{\rho_e t_e + R_{ct}^c + R_{ct}^a}(-E - \phi_{II}^a(r) + \phi_{II}^c(r)) = 0 \tag{21}$$

Expanding Eq. (21), rearranging terms, and factoring out terms in Δr gives

$$-\frac{r}{\Delta r}\left[\frac{\phi_{II}^c(r+\Delta r) - \phi_{II}^c(r)}{\Delta r} - \frac{\phi_{II}^c(r) - \phi_{II}^c(r-\Delta r)}{\Delta r}\right] - \frac{\phi_{II}^c(r+\Delta r) - \phi_{II}^c(r-\Delta r)}{2\Delta r} + rk_c(-E - \phi_{II}^a(r) + \phi_{II}^c(r)) = 0 \tag{22}$$

where k_c is the same parameter as defined earlier. Taking the limit as $\Delta r \to 0$ gives the differential equation

$$-r\frac{d^2\phi_{II}^c(r)}{dr^2} - \frac{d\phi_{II}^c(r)}{dr} + rk_c(-E - \phi_{II}^a(r) + \phi_{II}^c(r)) = 0 \tag{23}$$

Differential Eq. (23) describes the spatial dependence of electrostatic potential within the cathode for the two-dimensional interconnect symmetry in the range $r_0 \le r \le R/2$. This equation involves the electrostatic potential within the anode as a function of position, which is not known. The governing equation for the anode is found in a similar manner, and is given by

$$-r\frac{d^2\phi_{II}^a(r)}{dr^2} - \frac{d\phi_{II}^a(r)}{dr} + rk_a(-E - \phi_{II}^c(r) + \phi_{II}^a(r)) = 0 \tag{24}$$

Differential Eqs. (23) and (24) are linearly independent and can be solved simultaneously to obtain $\phi_{II}^c(r)$ and $\phi_{II}^a(a)$. In order to reduce this system of two differential equations and two unknowns to a single differential equation involving only one unknown, the following substitution will be made

$$v_{II}(r) = \phi_{II}^c(r) - \phi_{II}^a(r) \tag{25}$$

Eq. (25) is the difference in electrostatic potentials between the cathode and the anode at a position, r. Subtracting Eq. (24) from Eq. (23), and making the above substitution gives

$$-\frac{d^2 v_{II}(r)}{dr^2} - \frac{1}{r}\frac{dv_{II}(r)}{dr} + (k_c + k_c)v_{II}(r) = (k_c + k_a)E \tag{26}$$

This equation differs from Eq. (9) by virtue of the presence of the term $(1/r)(dv_{II}(r)/dr)$. Eq. (26) can be identified as the modified Bessel equation [10,11]. The solution to this differential equation is given by [10,11]

$$v_{II}(r) = E + v_3 I_0(ar) + v_4 K_0(ar) \tag{27}$$

where $I_0(ar)$ and $K_0(ar)$ are the modified Bessel functions of zeroth-order of the first and second kind, respectively, and v_3 and v_4 are constants. The constants v_3 and v_4 can be found by applying the appropriate boundary conditions, namely,

$$v_{II}(r_0) = \phi^0 \quad \text{and} \quad \left.\frac{dv_{II}(r)}{dr}\right|_{r=R/2} = 0 \tag{28}$$

Again, the first boundary condition represents the fixed potential between the interconnect contacts. The second boundary condition is obtained by deducing that no current flows across the perimeter at $r = R/2$. It can be shown that the constants v_3 and v_4 are given by

$$v_3 = \frac{\phi^0 - E}{[I_0(ar_0) + \{I_1(aR/2)/K_1(aR/2)\}K_0(ar_0)]} \quad \text{and} \quad v_4 = v_3\frac{I_1(aR/2)}{K_1(aR/2)} \tag{29}$$

[2] This assumes t_i much larger than the thickness of interconnect away from the ribs.

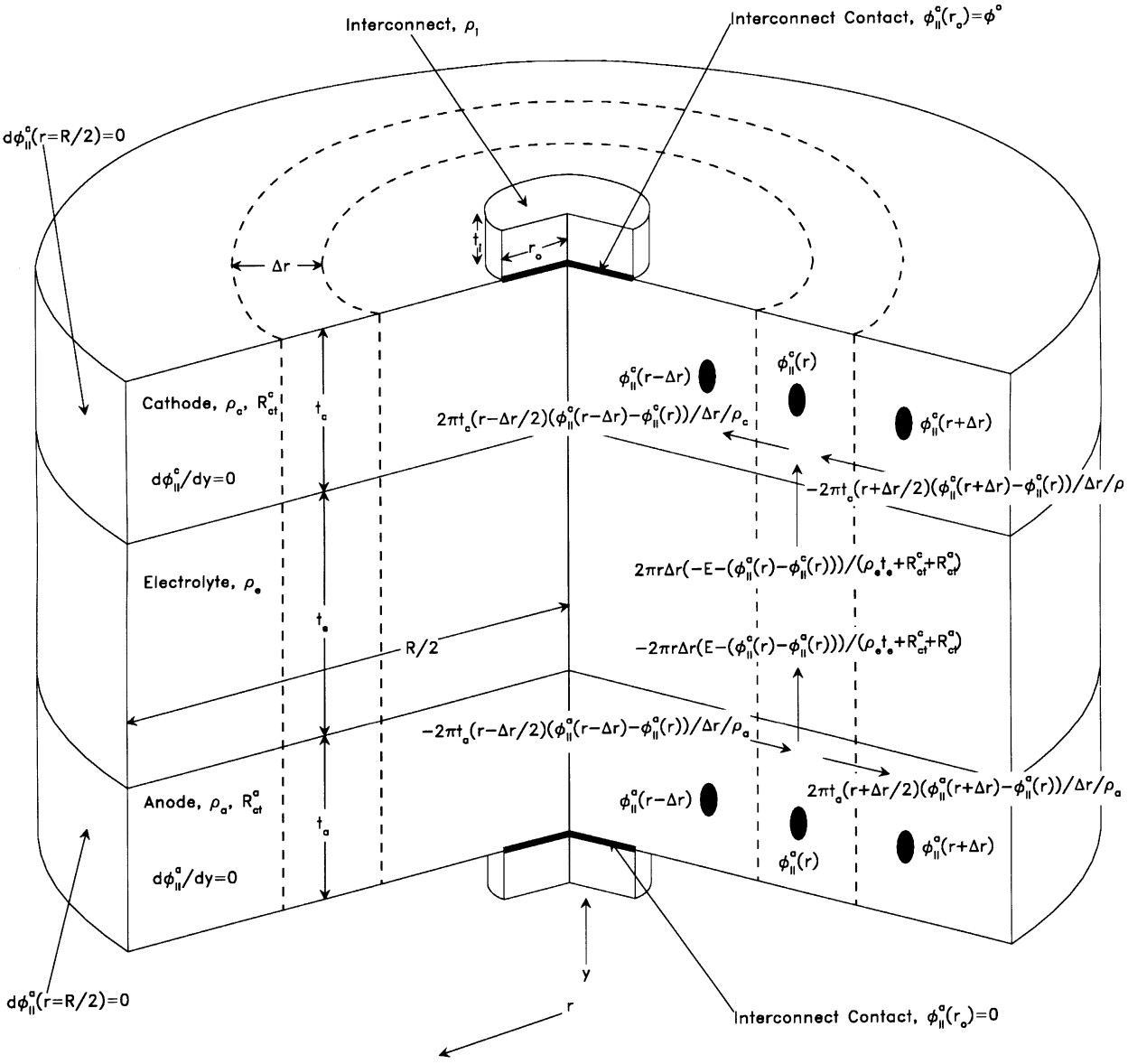

Fig. 4. A schematic showing a section of the SOFC depicted in Fig. 2. This circular section is obtained by approximating the hexagonal, in-plane repeat unit of the two-dimensional interconnect geometry with a circle of the same area.

and the complete solution for the potential drop across the cell as a function of position is given by

$$v_{II}(r)=E+(\phi^0-E)\left(\frac{I_0(ar)K_1(aR/2)+K_0(ar)I_1(aR/2)}{I_0(ar_0)K_1(aR/2)+K_0(ar_0)I_1(aR/2)}\right) \tag{30}$$

In the above equations, K_1 and I_1 are respectively modified Bessel functions of first-order, and of first and second kind. Eq. (30) may be used as an intermediate result to obtain solutions for $\phi^c_{II}(r)$ and $\phi^a_{II}(r)$. Alternatively, it is sufficient for the evaluation of the area-specific resistance of the repeat unit.

Examination of Fig. 4 shows that there are two separate regions of the cell that contribute to the total current flow, I_{II}. For the inner region located directly beneath the interconnect contact, that is $0 \le r \le r_0$, the potential difference is constant, and the current flowing is given by

$$I^i_{II}=\frac{(E-\phi^0)\pi r_0^2}{\rho_e t_e+R^c_{ct}+R^a_{ct}} \tag{31}$$

In the outer region, that is $r_0 \le r \le R/2$ the difference in potentials between the cathode and the anode varies as a function of position. The current flow through a ring of the electrolyte is given by

$$dI^0_{II}(r)=\frac{2\pi r(E-v_{II}(r))\,dr}{\rho_e t_e+R^c_{ct}+R^a_{ct}} \tag{32}$$

Substitution for $v_{II}(r)$ from Eq. (30) in the above equation, and integration between r_0 and $R/2$ gives the corresponding current, given by

$$I_{II}^0 = \left(\frac{2\pi r_0(E-\phi^0)}{a(\rho_e t_e + R_{ct}^c + R_{ct}^a)}\right) \times \left(\frac{K_1(ar_0)I_1(aR/2) - I_1(ar_0)K_1(aR/2)}{K_0(ar_0)I_1(aR/2) + I_0(ar_0)K_1(aR/2)}\right) \quad (33)$$

The net current flowing through the electrolyte across area of $\pi R^2/4$ is given by

$$I_{II} = I_{II}^i + I_{II}^0 \quad (34)$$

The resistance of the structure shown in Fig. 4, for a pair of opposite interconnect contacts, and the corresponding area, is given by applying Ohm's law, i.e. $d\phi^0/dI_{II}$. The interconnect material contributes a resistance of $\rho_i t_i/(\pi r_0^2)$, to the total.[3] Multiplying the total resistance by the area, $\pi R^2/4$, gives an analytical expression for the area-specific resistance (ASR) of the stack per one repeat unit, and is given by

$$R_{II} = \frac{R^2}{4}\left(\frac{\rho_e t_e + R_{ct}^c + R_{ct}^a}{r_0^2 + (2r_0/a)[\{K_1(ar_0)I_1(aR/2) - I_1(ar_0)K_1(aR/2)\}/\{K_0(ar_0)I_1(aR/2) + I_0(ar_0)K_1(aR/2)\}]} + \frac{\rho_i t_i}{r_0^2}\right) \quad (35)$$

Note that this is a function of the various material and design parameters.

3. Results and discussion

Eqs. (19) and (35) give the area-specific resistances (ASR) in terms of transport and design parameters of a SOFC stack-repeat unit for one- and two-dimensional interconnect symmetries. They show that it is not possible to design an interconnect independent of cell parameters since the overall area-specific resistance depends upon a number of parameters pertaining to the cell. Two types of planar cell designs are currently under investigation at several laboratories: (1) thick YSZ electrolyte as the support member with thin electrodes, screen-printed onto the electrolyte, and (2) thin YSZ electrolyte-supported on a thick porous anode with a cathode of intermediate thickness. In what follows, calculations are presented for typical values of various parameters for both types of cells. We will refer to these as an electrolyte-supported cell and an anode-supported cell, respectively. The parameters chosen for the electrolyte-supported cell are: $\rho_e = 50\,\Omega$ cm, $t_e = 150\,\mu$m, $\rho_c = 0.1\,\Omega$ cm, $t_c = 25\,\mu$m, $R_{ct}^c = 0.2\,\Omega\,cm^2$, $\rho_a = 0.001\,\Omega$ cm, $t_a = 25\,\mu$m, and $R_{ct}^a = 0.1\,\Omega\,cm^2$. The interconnect contact dimension is selected as x_0 or $r_0 = 10\,\mu$m. The parameters chosen for the anode-supported cell are: $\rho_e = 50\,\Omega$ cm, $t_e = 10\,\mu$m, $\rho_c = 0.1\,\Omega$ cm, $t_c = 100\,\mu$m, $R_{ct}^c = 0.2\,\Omega\,cm^2$, $\rho_a = 0.001\,\Omega$ cm, μm, and $R_{ct}^a = 0.1\,\Omega\,cm^2$. All transport parameters are chosen to be the same for the two types of cells. The charge transfer resistances depend upon the intrinsic charge transfer characteristics (such as that occurring at a three phase boundary, TPB) and the microstructure (e.g. the TPB length). The calculations given here assume that the conductivity of the interconnect material is much greater than any component of the cell. If this is not the case, the term corresponding to the resistance of the interconnect material must be included.

Figs. 5 and 6 are plots of the calculated area-specific resistance for one- and two-dimensional interconnect symmetries as a function of the spacing between contacts, L or R, for the electrolyte- and anode-supported cells, respectively. It can be seen from the plots that regardless of the interconnect contact spacing, the one-dimensional symmetry always gives a lower area-specific resistance than the two-dimensional symmetry, consistent with expectations. For closely spaced interconnect contacts, the area-specific resistance is approximately equal to the single-cell resistance, $\rho_e t_e + R_{ct}^c + R_{ct}^a$. As the interconnect contact spacing is increased, a transition in behavior occurs. For large interconnect contact spacing, the area-specific resistance increases due to the resistance to flow of electrons in the

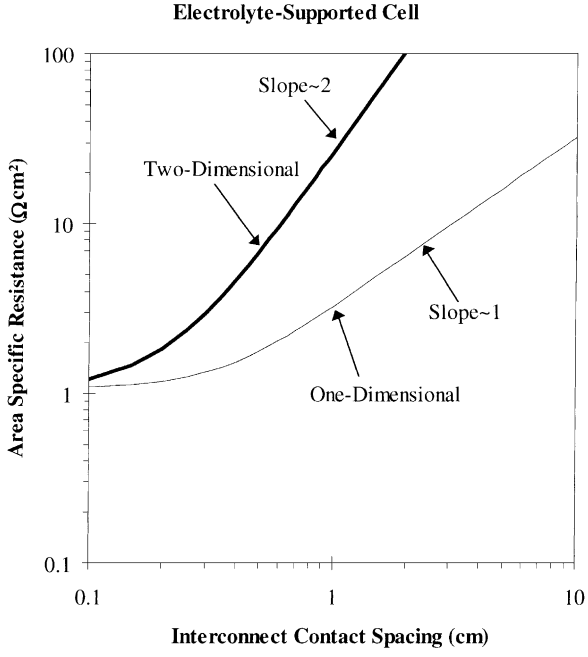

Fig. 5. Plots of the area-specific resistance (electrolyte-supported) for one- and two-dimensional interconnect geometries, respectively, as a function of spacing between the interconnect contacts, L or R. The values used in the calculation for an electrolyte-supported cell are: $\rho_e = 50\,\Omega$ cm, $t_e = 15\,\mu$m, $\rho_c = 0.1\,\Omega$ cm, $t_c = 25\,\mu$m, $R_{ct}^c = 0.2\,\Omega\,cm^2$, $\rho_a = 0.001\,\Omega$ cm, $t_a = 25\,\mu$m, $R_{ct}^a = 0.1\,\Omega\,cm^2$, and x_0 or $r_0 = 10\,\mu$m.

[3] This assumes that t_i is much greater than interconnect thickness away from the dimples.

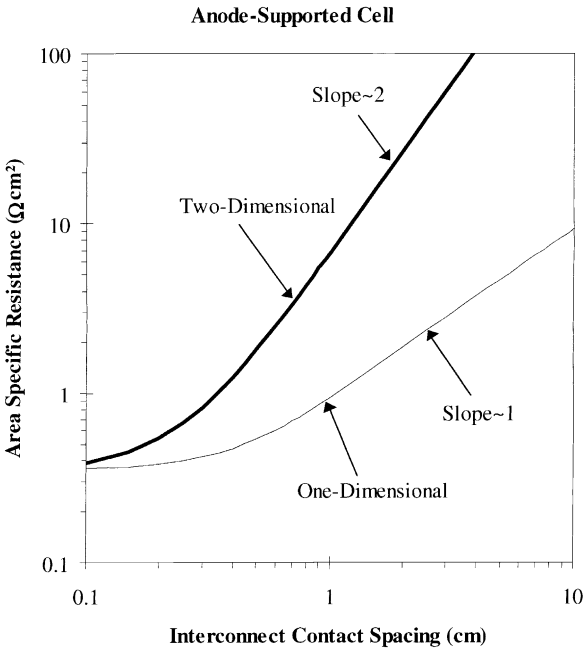

Fig. 6. Plots of the area-specific resistance (anode-supported) for one- and two-dimensional interconnect geometries, respectively, as a function of spacing between the interconnect contacts, L or R. The values used in the calculation for an anode-supported cell are: $\rho_e = 50\,\Omega$ cm, $t_e = 10\,\mu$m, $\rho_c = 0.1\,\Omega$ cm, $t_c = 100\,\mu$m, $R^c_{ct} = 0.2\,\Omega\,cm^2$, $\rho_a = 0.001\,\Omega$ cm, $t_a = 500\,\mu$m, $R^a_{ct} = 0.1\,\Omega\,cm^2$, and x_0 or $r_0 = 10\,\mu$m.

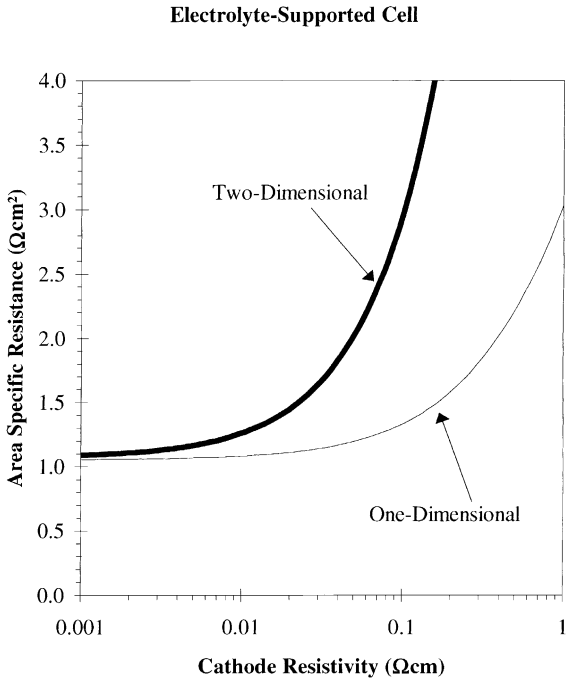

Fig. 7. Plots of the area-specific resistance (electrolyte-supported) for one- and two-dimensional interconnect geometries, respectively, as a function of cathode resistivity, ρ_c. The values used in the calculation for an electrolyte-supported cell are: $\rho_e = 50\,\Omega$ cm, $t_e = 150\,\mu$m, $t_c = 25\,\mu$m, $R^c_{ct} = 0.2\,\Omega\,cm^2$, $\rho_a = 0.001\,\Omega$ cm, $t_a = 25\,\mu$m, $R^a_{ct} = 0.1\,\Omega\,cm^2$, x_0 or $r_0 = 10\,\mu$m, and L or $R = 3$ mm.

electrocatalyst materials within the electrodes, i.e. electrode sheet resistance. The transition from single-cell-dominated to interconnect design-dominated resistance occurs at a lower interconnect contact spacing for the two-dimensional symmetry. The plot of Eq. (19) for the one-dimensional symmetry shows that for widely spaced interconnect contacts, the area-specific resistance increases linearly with interconnect contact spacing, L. By comparison, the plot of Eq. (35) for the two-dimensional symmetry shows that for widely spaced interconnect contacts, the area-specific resistance increases parabolically with interconnect contact spacing, R. Also, interconnect contact spacing for designs with a two-dimensional symmetry must be smaller than for designs with a one-dimensional spacing to achieve the same area-specific resistance. As a numerical example, if the desired maximum repeat unit ASR is $0.5\,\Omega\,cm^2$ for anode-supported cell design (Fig. 6), the interconnect contact spacing for two-dimensional geometry must be under 2 mm (<0.2 cm), while that for the one-dimensional geometry can be as large as ~5 mm (~0.5 cm).

Comparison of Figs. 5 and 6 also shows that for the same transport properties, the anode-supported cell exhibits a lower area-specific resistance than the electrolyte-supported cell. This, of course, is to be expected, as the electrolyte resistance is higher in the case of electrolyte-supported cells.

In the calculations given in Figs. 5 and 6, the cathode resistivity was assumed to be 0.1 Ω cm. The typical value of LSM is about 0.01 Ω cm. However, as the cathode is porous, generally contains some YSZ, and that its conductivity can be lower in oxygen-depleted air, such as during the actual SOFC operation, the actual cathode resistivity may be much higher than 0.01 Ω cm, hence, the choice of 0.1 Ω cm. Further, if LSM reacts with YSZ to form $La_2Zr_2O_7$, the resistivity may be even higher than 0.1 Ω cm. However, if the cathode consists of materials such as cobaltites, and their reaction with YSZ can be suppressed (by using a ceria buffer layer) the resistivity could be much lower than 0.01 Ω cm. Thus, for the purposes of evaluating the role of cathode resistivity, calculations of the area-specific resistance (ASR) were made over a range of cathode resistivities, for both electrolyte-supported and anode-supported cells, and for both interconnect geometries, for an interconnect contact spacing of 3 mm, and interconnect contact dimension of 10 μm. The results of these calculations are shown in Figs. 7 and 8. Note that as the cathode resistivity rises, the ASR rises; and once again, it rises faster for the two-dimensional symmetry. For the two-dimensional geometry, in particular, the rise in ASR is rather rapid, emphasizing the importance of the need for a low sheet resistance. For the anode-supported design (Fig. 8), which has lower overall ASR compared to the electrolyte-supported design, note that the repeat unit ASR for the two-dimensional geometry increases from ~0.4 $\Omega\,cm^2$ for $\rho_c = 0.01\,\Omega$ cm, to ~0.8 $\Omega\,cm^2$ for $\rho_c = 0.1\,\Omega$ cm. That is, the stack performance drops by a factor of 2. Beyond $\rho_c = 0.1\,\Omega$ cm, the rise is even more rapid. Over the same range, the one-dimensional geometry is more forgiving.

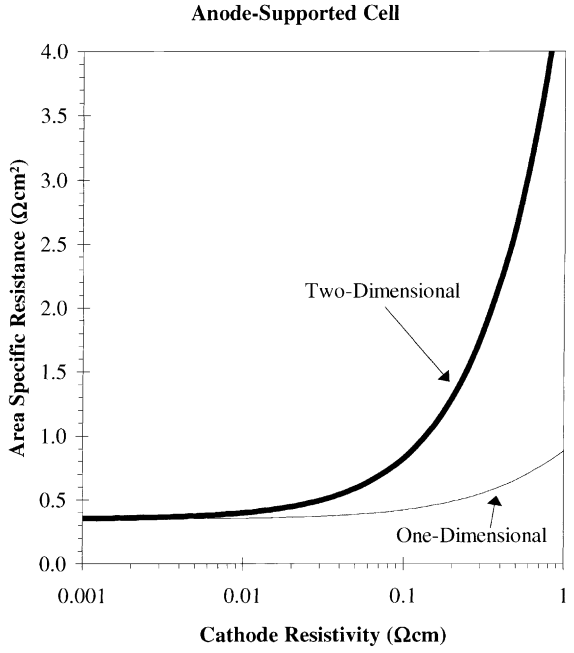

Fig. 8. Plots of the area-specific resistance (anode-supported) for one- and two-dimensional interconnect geometries, respectively, as a function of cathode resistivity, ρ_c. The values used in the calculation for an anode-supported cell are: $\rho_e = 50\,\Omega$ cm, $t_e = 10\,\mu$m, $t_c = 100\,\mu$m, $R^c_{ct} = 0.2\,\Omega\,\text{cm}^2$, $\rho_a = 0.001\,\Omega$ cm, $t_a = 500\,\mu$m, $R^a_{ct} = 0.1\,\Omega\,\text{cm}^2$, x_0 or $r_0 = 10\,\mu$m, and L or $R = 3$ mm.

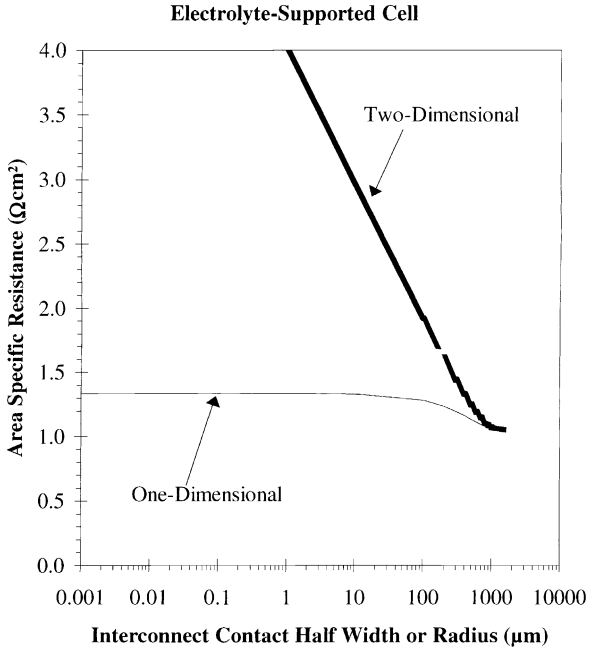

Fig. 9. Plots of the area-specific resistance (electrolyte-supported cell) for one- and two-dimensional interconnect geometries, respectively, as a function of interconnect contact half-width or radius, x_0 or r_0. The values used in the calculation for an electrolyte-supported cell are: $\rho_e = 50\,\Omega$ cm, $t_e = 150\,\mu$m, $\rho_c = 0.1\,\Omega$ cm, $t_c = 25\,\mu$m, $R^c_{ct} = 0.2\,\Omega\,\text{cm}^2$, $\rho_a = 0.001\,\Omega$ cm, $t_a = 25\,\mu$m, $R^a_{ct} = 0.1\,\Omega\,\text{cm}^2$, L or $R = 3$ mm.

Figs. 9 and 10 are plots of the calculated area-specific resistance for one- and two-dimensional symmetries as a function of the interconnect contact half-width or radius, x_0 or r_0, for stacks with electrolyte-supported and anode-supported cells, respectively, for interconnect contact spacing of 3 mm. Once again, it can be seen from the figures that the area-specific resistance for the interconnect contact design with a one-dimensional symmetry is always lower than the design with a two-dimensional symmetry. For large interconnect contact areas, the area-specific resistance is approximately equal to the single-cell resistance,[4] $\rho_e t_e + R^c_{ct} + R^a_{ct}$, and as the contact area decreases, the area-specific resistance increases. The area-specific resistance for one-dimensional symmetry increases to an asymptotic maximum as the contact half-width (area) decreases. An examination of Eq. (19) shows that for a highly conducting interconnect material ($\rho_i \to 0$), and small rib thickness ($t_i \to 0$), the second term in parenthesis can be neglected. In all calculations presented here, this assumption was made. If now one examines the limit $x_0 \to 0$, the repeat unit ASR becomes

$$R_I = \frac{aL(\rho_e t_e + R^c_{ct} + R^a_{ct})}{2[(1 - e^{-aL})/(1 + e^{-aL})]} \tag{36}$$

[4] Of course, interconnect contact area cannot be increased indefinitely, otherwise there would be no space left for the transport of gaseous species along the interconnect faces.

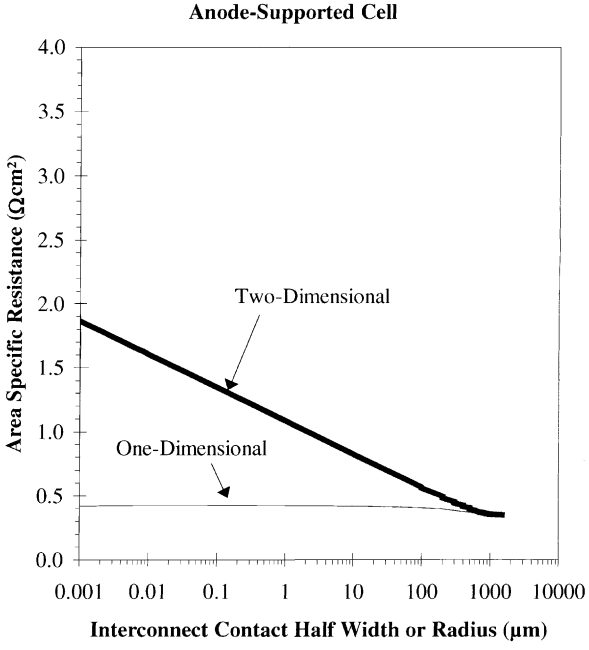

Fig. 10. Plots of the area-specific resistance (anode-supported cell) for one- and two-dimensional interconnect geometries, respectively, as a function of interconnect contact half-width or radius, x_0 or r_0. The values used in the calculation for an anode-supported cell are: $\rho_e = 50\,\Omega$ cm, $t_e = 10\,\mu$m, $\rho_c = 0.1\,\Omega$ cm, $t_c = 100\,\mu$m, $R^c_{ct} = 0.2\,\Omega\,\text{cm}^2$, $\rho_a = 0.001\,\Omega$ cm, $t_a = 500\,\mu$m, $R^a_{ct} = 0.1\,\Omega\,\text{cm}^2$, L or $R = 3$ mm.

That is, the ASR approaches a finite value. A similar analytical expression of the limit of Eq. (35) as $r_0 \to 0$, is difficult to obtain. It can be shown, however, that as $r_0 \to 0$, both $K_0(ar_0)$ and $K_1(ar_0)$ approach infinity, with $K_1(ar_0)$ rising faster. If the ratio $K_1(ar_0)/K_0(ar_0)$ rises slower than $1/r_0$, one would expect the limit of Eq. (35) to approach infinity as $r_0 \to 0$. Numerical calculations given in Figs. 9 and 10 show at the ASR monotonically increases as r_0 decreases. That is, the area-specific resistance for a two-dimensional symmetry does not increase to a finite maximum as the contact area decreases. In fact, Eq. (35) for the two-dimensional area-specific resistance is singular, i.e. infinite, in the limit as the contact radius, r_0 approaches zero. Thus, the interconnect contact design with a two-dimensional symmetry can have a significantly higher area-specific resistance than the design with a one-dimensional symmetry in cases where the contact area is small and the spacing between contacts is large. Generally, however, the interconnect contact dimension is expected to be larger than 10 μm. Thus, the interconnect contact dimension is not expected to exhibit a large effect. However, in an actual SOFC stack, due to dimensional irregularities, it can often so happen that the contact between cell and interconnect may not be perfect. This may lead to a situation where in some of the regions, interconnect may not be in contact with the cell. This would be equivalent to locally increasing L or R, and thus, effectively increasing the ASR. The analysis presented here shows that the adverse effect of irregular contact in general would be greater in the case of two-dimensional geometry than in the case of one-dimensional geometry.

The interconnect contact spacing at which area-specific resistance (ASR) transitions from single-cell dominated to sheet (electrode) resistance dominated can be estimated from Eq. (11). For interconnect spacing wider than $\sim 1/a$, resistance to distribution of current in the electrodes begins to become larger than the resistance of the single-cell, $\rho_e t_e + R^c_{ct} + R^a_{ct}$. In fact, the parameter $1/a$ arises independent of the boundary conditions or shape of the single-cells. As a general rule or a design guideline, the spacing between the interconnect contacts should be less than $1/a$ so that performance of the stack reflects performance of the single-cells. The Siemens–Westinghouse fuel cell design modeled by Bessette et al. can be approximately described in terms of the one-dimensional interconnect geometry and analyzed in terms of the parameter $1/a$ [9]. An analytical expression for the area-specific resistance similar to Eq. (19) can be obtained by applying slightly different boundary conditions to the general solutions for potential as a function of position. The cell parameters used by Bessette et al. are as follows: $\rho_e = 9.98\ \Omega$ cm, $t_e = 40$ μm, $\rho_c = 0.013\ \Omega$ cm, $t_c = 7000$ μm (0.7 cm), $R^c_{ct} + R^a_{ct} = 0.7\ \Omega\ \text{cm}^2$ (estimate), $\rho_a = 0.001\ \Omega$ cm, and $t_a = 100$ μm. For these parameters, the value of $1/a$ is 2.42 cm. The diameter of the tube on which the single-cell is built was assumed to be 11 cm in the work of Bessette et al. [9]. Of the circumference, ~28.4 cm is active electrolyte, and the repeat unit length consistent with the one-dimensional interconnect symmetry is half this value, 14.2 cm. Thus, the internal resistance of the tube-based design assumed in the calculations by Bessette et al. is dominated by sheet resistance in the electrodes [9]. Reduction of the diameter of the tubes to less than 1.5 cm and increase in thickness of the electrode should give significantly lower area-specific resistance.

For the calculations presented in Figs. 5–8, the chosen charge transfer resistances correspond to composite electrodes that are mixtures of an electrocatalyst and an oxygen ion conductor. For the cathode, for example, a suitable mixture is that of Sr-doped $LaMnO_3$ (LSM) and YSZ. For the anode, a suitable mixture is Ni + YSZ. A porous composite electrode that consists of a contiguous mixture of an electrocatalyst and an ionic conductor exhibits a much lower overall charge transfer resistance than a single-phase, electronically conducting electrocatalyst (e.g. LSM). This improved performance of a composite electrolyte is largely due to increased TPB length, which leads to a spreading of the reaction zone into the electrode. Distance to which this spreading occurs depends upon a number of parameters, including the microstructure. In general, the finer the microstructure, the lower is the overall charge transfer resistance, the better is the performance, and the smaller is the required thickness of the electrode (from the standpoint of lower polarization).

Recent work has shown that in terms of the intrinsic charge transfer resistance of the cathode, $R^c_{ct(0)}$, which for example describes electrocatalytic behavior of LSM (of a given LSM particle size and particle number density per unit area of YSZ) on YSZ, the effective charge transfer resistance of a composite cathode comprising a porous mixture of LSM and YSZ, namely, R^c_{ct}, is given by [3,6]

$$R^c_{ct} \approx \sqrt{\frac{d_c \rho^c_e R^c_{ct(0)}}{1 - p_c}} \tag{37}$$

where p_c is the cathode porosity, ρ^c_e is the ionic resistivity of the composite cathode (that of the YSZ in the composite cathode), and d_c is the particle size of the YSZ in the composite cathode. The above equation is applicable typically for cathode thicknesses in excess of a critical thickness, λ, defined by [6]

$$\lambda = \sqrt{\frac{d_c R^c_{ct(0)}(1 - p_c)}{\rho^c_e}} \tag{38}$$

More specifically, Eq. (37) is applicable if the electrode thickness is greater than about two or three times λ. The typical grain size of YSZ in the LSM–YSZ cathode is $d_c \sim 1$ micron. For a typical volume fraction of LSM (~0.5) and particle size (~1 μm), an approximate value of $R^c_{ct(0)}$ at 800 °C is about $1\ \Omega\ \text{cm}^2$. Finally, for YSZ in the cathode, the ionic resistivity, ρ^c_e is about $50\ \Omega$ cm. For a cathode porosity of ~0.3, using the values mentioned here, Eq. (38) gives $\lambda \approx 12$ microns. Thus, a minimum cathode thickness

of ∼20 to 30 microns ensures the applicability of Eq. (37). A similar equation is also applicable for the anode. For the calculations presented here, therefore, R_{ct}^{c} and R_{ct}^{a} correspond to composite electrodes.

For the present calculations, the charge transfer reactions are assumed to occur at the physically distinct cathode–electrolyte and anode–electrolyte interfaces. This, of course, is not strictly correct since the very nature of composite electrodes allows for the occurrence of charge transfer reactions throughout the electrode. In this simplified, but analytical approach, however, it is assumed to occur at the physically distinct electrolyte/electrode interface. This is justified as long as λ is much less than t_c.

4. Conclusions

The effects of interconnect contact spacing and contact area, in conjunction with transport properties and design parameters of a single-cell on overall SOFC stack resistance were investigated. Area-specific resistance (ASR) of cell-interconnect repeat unit was used as the figure of merit for the purposes of comparison. Analytical expressions for the ASR for interconnect geometries with one- and two-dimensional symmetries were derived using a ladder network approach. The advantage of analytical expressions over numerical models is that it is in principle possible to explicitly evaluate the role of various parameters on the overall stack resistance to assist in the optimization of stack performance. The analytical results then may guide a detailed numerical modeling effort. While the one-dimensional symmetry is expected to give a lower resistance than the two-dimensional symmetry, the present analysis gives closed form analytical expressions, which allow for a quantitative comparison between the two. For an interconnect design with a one-dimensional symmetry, the area-specific resistance (ASR) was found to increase linearly as a function of the interconnect spacing for widely spaced interconnect contacts, and the size of the interconnect contact area had only a minor effect. The area-specific resistance (ASR) for an interconnect design with a two-dimensional symmetry, on the other hand, was found to increase parabolically as a function of interconnect contact spacing for widely spaced interconnects and was found to be singular (infinite) at zero interconnect contact area. Thus, interconnects with widely spaced contacts of a small contact area should be avoided when an interconnect design when a two-dimensional symmetry is used. Two designs of single cells were considered and compared, electrolyte- and anode-supported. Regardless of the interconnect design symmetry or whether electrolyte- or anode-supported cells are used to build a SOFC stack, the area-specific resistance (ASR) begins to rise rapidly due to sheet resistance within the electrodes for interconnect contact spacing greater than 5 mm for the values of parameters used in the present calculations. The best design was found to be the one having anode-supported cells with closely spaced interconnect contacts and a one-dimensional symmetry.

Acknowledgements

This work was supported by the Gas Research Institute under contract #50942603276.

References

[1] S. de Souza, S.J. Visco, L.C. De Jonghe, Reduced-temperature solid oxide fuel cell based on YSZ thin-film electrolyte, J. Electrochem. Soc. 141 (3) (1997) L35–L37.
[2] J.W. Kim, A.V. Virkar, K.Z. Fung, K. Mehta, S.C. Singhal, Polarization effects in intermediate temperature anode-supported solid oxide fuel cell, J. Electrochem. Soc. 146 (1) (1999) 69–78.
[3] A.V. Virkar, J. Chen, C.W. Tanner, J.W. Kim, The role of electrode microstructure on activation and concentration polarizations in solid oxide fuel cells, Solid State Ionics 131 (1–2) (2000) 189–198.
[4] T. Kenjo, S. Osawa, K. Fujikawa, High-temperature air cathodes containing ion conductive oxides, J. Electrochem. Soc. 138 (2) (1991) 349–355.
[5] T. Kenjo, M. Nishiya, $LaMnO_3$ air cathodes containing ZrO_2 electrolyte for high-temperature solid oxide fuel cells, Solid State Ionics 57 (3–4) (1992) 295–302.
[6] C.W. Tanner, K.Z. Fung, A.V. Virkar, The effect of porous composite electrode structure on solid oxide fuel cell performance. I. Theoretical analysis, J. Electrochem. Soc. 144 (1) (1997) 21–30.
[7] E.F. Sverdrup, C.J. Warde, R.L. Eback, Design of high-temperature solid-electrolyte fuel cell batteries for maximum power output per unit volume, Energy Conversion 13 (1973) 129.
[8] S. Ahmed, C. McPheeters, R. Kumar, Thermal–hydraulic model of a monolithic solid oxide fuel cell, J. Electrochem. Soc. 138 (9) (1991) 2712–2718.
[9] N.F. Bessette, W.J. Wepfer, J. Winnick, A mathematical model of a solid oxide fuel cell, J. Electrochem. Soc. 142 (11) (1995) 3792–3800.
[10] C.R. Wylie, Advanced Engineering Mathematics, McGraw-Hill, New York, 1975, p. 403.
[11] M. Abramowitz, I.A. Stegun, Handbook of Mathematical Functions, Dover, New York, 1972, p. 374.